

Separate tuning of nematicity and spin fluctuations to unravel the origin of superconductivity in FeSe

Seung-Ho Baek,^{1,*} Jong Mok Ok,^{2,3} Jun Sung Kim,^{2,3} Saicharan Aswartham,⁴
Igor Morozov,^{4,5} Dmitriy Chareev,^{6,7,8} Takahiro Urata,^{9,10} Katsumi
Tanigaki,⁹ Yoichi Tanabe,^{9,11} Bernd Büchner,^{4,12} and Dmitri V. Efremov⁴

¹*Department of Physics, Changwon National University, Changwon 51139, Korea*

²*Department of Physics, Pohang University of
Science and Technology, Pohang 790-784, Korea*

³*Center for Artificial Low Dimensional Electronic Systems,
Institute of Basic Science, Pohang 790-784, Korea*

⁴*IFW Dresden, Helmholtzstr. 20, 01069 Dresden, Germany*

⁵*Moscow State University, Moscow 119991, Russia*

⁶*Institute of Experimental Mineralogy,
Russian Academy of Sciences, 142432, Russia*

⁷*Ural Federal University, Ekaterinburg 620002, Russia*

⁸*Kazan Federal University, Kazan 420008, Russia*

⁹*Department of Physics, Graduate School of Science,
Tohoku University, Sendai 980-8578, Japan*

¹⁰*Department of Materials Physics, Nagoya University,
Chikusa-ku, Nagoya 464-8603, Japan*

¹¹*Department of Science, Okayama University of Science, Okayama 700-0005, Japan*

¹²*Department of Physics, Technische Universität Dresden, 01062 Dresden, Germany*

(Dated: September 16, 2021)

Abstract

The interplay of orbital and spin degrees of freedom is the fundamental characteristic in numerous condensed matter phenomena, including high temperature superconductivity, quantum spin liquids, and topological semimetals. In iron-based superconductors (FeSCs), this causes superconductivity to emerge in the vicinity of two other instabilities: nematic and magnetic. Unveiling the mutual relationship among nematic order, spin fluctuations, and superconductivity has been a major challenge for research in FeSCs, but it is still controversial. Here, by carrying out ^{77}Se nuclear magnetic resonance (NMR) measurements on FeSe single crystals, doped by cobalt and sulfur that serve as control parameters, we demonstrate that the superconducting transition temperature T_c increases in proportion to the strength of spin fluctuations, while it is independent of the nematic transition temperature T_{nem} . Our observation therefore directly implies that superconductivity in FeSe is essentially driven by spin fluctuations in the intermediate coupling regime, while nematic fluctuations have a marginal impact on T_c .

Introduction

In correlated Fermi fluids, nematicity refers to the state in which rotational symmetry is spontaneously broken, while time-reversal invariance is preserved, and consequently, the symmetry of the crystal changes from tetragonal to orthorhombic.¹ An important aspect in iron-based superconductors (FeSCs) is the propensity for nematic ordering, which is usually followed by a spin-density-wave (SDW) transition, near a superconducting (SC) dome.²⁻⁴ Regardless of the origin of nematicity that is still under debate,^{5,6} this raises the fundamental issue of whether superconductivity in FeSCs is closely related to nematicity^{7,8} or magnetism^{9,10} or both.¹¹ To address this issue, it is much desirable to separate nematic order from magnetic one. In this respect, FeSe has been a key platform for studying the origin of nematicity and its role in superconductivity,¹² as it exhibits nematic and SC orders at well separated temperatures, $T_{\text{nem}} \sim 90$ K and $T_c \sim 9$ K, respectively, without involving magnetic order. Numerous recent studies in FeSe show that nematicity causes the strongly anisotropic SC gap symmetry,¹³⁻¹⁶ and further discuss that nematic fluctuations might play an important role for the superconducting pairing mechanism.^{17,18} On the other hand, the leading role of spin fluctuations (SFs) in the SC mechanism of FeSe, as in other FeSCs whose parent materials magnetically orders, has been also proposed in the literature.¹⁹⁻²² In this spin fluctuation-mediated pairing scenario, the subsequent question arises whether weak or strong coupling approach is appropriate to establish theory of superconductivity in FeSCs. It is quite interesting to note that recent NMR studies of FeSe under high pressure reveal the persistence of local nematicity at temperatures far above T_{nem} , which suggests a correlation between local nematicity and magnetism.^{23,24} Another interesting observation by NMR is the unusual suppression of $(T_1T)^{-1}$ at optimal pressure,²⁵ suggesting that the interplay of SFs and superconductivity may undergo a critical change with high pressure.

As a system undergoes a nematic transition ($C_4 \rightarrow C_2$), two nematic domains are naturally formed below T_{nem} , still preserving the C_4 symmetry on average. Accordingly, it is usually required to detwin nematic domains, for example, by an external strain to study nematicity. As a local probe in real space, on the other hand, NMR is uniquely capable of observing the two nematic domains at the same time. Indeed, it has been established that the splitting of the NMR line in FeSCs at an external field H applied along the crystallographic a axis represents the nematic order parameter and its onset temperature corresponds

to the nematic transition temperature T_{nem} (Ref. 26–28, see Fig. 1c). In order to investigate whether and how nematicity is related to superconductivity, we measured the ^{77}Se line splitting for $H_{\parallel a}$ in $\text{FeSe}_{1-y}\text{S}_y$ and $\text{Fe}_{1-x}\text{Co}_x\text{Se}$ single crystals. In general, it is considered that substituting isovalent S for Se is equivalent to the application of (negative) chemical pressure, and Co substituted for Fe supplies an additional electron and also plays as a paramagnetic impurity. Therefore, a systematic NMR study on the two different doped systems may enable a full understanding of the relationship between nematicity, magnetism, and superconductivity.

Results and Discussion

Figure 1 shows how the temperature dependence of the ^{77}Se NMR spectrum in FeSe is modified as a function of x in $\text{Fe}_{1-x}\text{Co}_x\text{Se}$ (Figs. 1a and 1b) and as a function of y in $\text{FeSe}_{1-y}\text{S}_y$ (Figs. 1d and 1e). For $\text{FeSe}_{1-y}\text{S}_y$, we find that the onset temperature of the line splitting or T_{nem} is gradually suppressed, consistent with previous studies.^{17,21} For $\text{Fe}_{1-x}\text{Co}_x\text{Se}$, however, T_{nem} hardly changes for $x = 0.018$. Upon further doping to slightly higher $x = 0.025$, the ^{77}Se line becomes significantly broad, making difficult to identify the onset of the line splitting. The much larger ^{77}Se line broadening for Co doping than for S doping is well understood because Co has a strong influence on Fe moments as a nonmagnetic impurity. We notice, however, that the ^{77}Se line broadening is not simply proportional to the concentration of Co dopants, but rather it appears to increase drastically above $x \sim 0.025$. In fact, for $x = 0.036$, it is not possible to observe the line splitting anymore, because the linewidth is much larger than the nematic splitting (see supplementary Fig. 1). On the other hand, the ^{77}Se linewidth is proportional to both S and Co dopants similarly, as long as Co-doping is smaller than 2.5%, as shown in supplementary Fig. 2. This suggests that doped Co impurities beyond $\sim 2.5\%$ of Fe sites causes a strong disorder effect on the correlation between Fe spins, indicating the existence of a critical doping level above which the magnetic correlation length becomes sufficiently long to induce a short-range exchange.

Although T_{nem} cannot be accurately determined for $x = 0.025$ due to the large line broadening in the nematic state, we clearly observed the line splitting below 80 K, as shown in Fig. 1a. While this puts a lower limit of T_{nem} , the fitting analysis of ^{77}Se spectra in Fig. 1a also suggests that the line splitting seems to persist even up to 100 K (see vertical

bars). (The detailed Knight shift data as a function of temperature and doping are shown in supplementary Fig. 3.) This suggests that Co impurities may induce a spatial distribution of T_{nem} in the temperature range, $80 \leq T_{\text{nem}} \leq 100$ K. Regardless of details, T_{nem} is marginally suppressed by Co doping within the doping range investigated, as shown in Fig. 2a. Note that the Co doping range investigated is very narrow, and thus we are unable to argue whether T_{nem} remains a constant at higher Co-doping. In any case, Figs. 2a and 2b reveal that T_{nem} and T_c are clearly decoupled.

Interestingly, the split ^{77}Se lines below 80 K for $x = 0.025$ is notably anisotropic, i.e., the peak for the lower frequency side is broader than that for the higher frequency. The origin of the anisotropic line shape is unclear, but we note that the similar anisotropic ^{77}Se line shape is also observed at $T < 20$ K for $x = 0.018$ (see Fig. 1b). This implies that magnetic inhomogeneity, which otherwise appears at low temperatures, prevails at higher temperatures with higher Co doping.

Contrasting sharply with the weak dependence of nematicity on both S and Co dopants, our susceptibility measurements reveal that superconductivity is strongly dependent only on Co dopants. That is, T_c is rapidly suppressed by small Co doping, whereas it is robust with regard to S doping, as shown in Figs. 2a and 2b, being consistent with previous studies.^{29,30} The very different behavior of T_{nem} and T_c with doping indicates that nematic and superconducting orders are not directly coupled,^{31,32} raising a strong question as to whether nematicity and superconductivity are closely related.^{7,8,17,33}

Having established the lack of a coupling of the nematic and superconducting transition temperatures, we now discuss the role of SFs for superconductivity. For probing low energy SFs, we measured the spin-lattice relaxation rate, T_1^{-1} , as the quantity $(T_1 T)^{-1}$ is a measure of SFs at very low energy:

$$(T_1 T)^{-1} = \gamma_n^2 \lim_{\omega \rightarrow 0} \sum_{\mathbf{k}} A^2(\mathbf{k}) \frac{\chi''(\mathbf{k}, \omega)}{\omega}, \quad (1)$$

where $\chi''(\mathbf{k}, \omega)$ is the imaginary part of the dynamic susceptibility at momentum \mathbf{k} and frequency ω , γ_n is the nuclear gyromagnetic ratio, and $A(\mathbf{k})$ is the structure factor of the hyperfine interaction. Figures 2c and 2d show $(T_1 T)^{-1}$ as a function of Co and S doping, respectively, at $H_{\parallel a} = 9$ T. The data for the undoped FeSe crystal was taken from ref. 26. With increasing Co doping x in $\text{Fe}_{1-x}\text{Co}_x\text{Se}$, $(T_1 T)^{-1}$ or SFs above T_c is rapidly suppressed, which is in exact parallel with the suppression of T_c , as shown in Fig. 2a. Note that

for $x = 0.035$ superconductivity is completely absent, and correspondingly SFs are not enhanced at all at low temperatures. On the other hand, $(T_1T)^{-1}$ above T_c is unchanged with increasing S doping y in $\text{FeSe}_{1-y}\text{S}_y$ up to $y = 0.1$, as precisely T_c does (see Fig. 2b). From the data presented in Figure 2, therefore, one sees that T_c depends only on the strength of spin fluctuations, but not on T_{nem} . (At larger S-doping near $y = 0.2$, it was reported that both $(T_1T)^{-1}$ and T_c are strongly suppressed in such a way that the correlation between SFs and T_c persists,²¹ somewhat similar to the behavior in Co-doped samples.)

For further quantitative information on how SFs is related to T_c , we adopt a spin fluctuation model in the Eliashberg formalism,¹ or Millis-Monien-Pines (MMP) model.⁵ For this, we separate out the enhancement of $(T_1T)^{-1}$ that is solely associated with SFs from the data shown in Fig. 2c. Noting that $(T_1T)^{-1}$ for the non-superconducting sample ($x = 0.035$) approaches a constant, $(T_1T)_0^{-1} \equiv \Gamma_0$, without any enhancement at zero temperature, one may define the strength of SFs Γ for $H_{\parallel a}$ from the $(T_1T)^{-1}(x)$ values just above T_c :

$$\Gamma(x) \equiv (T_1T)^{-1}(x)|_{T_c} - \Gamma_0. \quad (2)$$

While the MMP model indicates that Γ is proportional to the square of the correlation length,⁵ $\xi^2(T)$, the estimation of the low energy part of the Eliashberg bosonic spectral function suggests that the coupling constant λ is proportional to ξ , i.e., $\sqrt{\Gamma}$. As it was analyzed by Radtke *et al.*³⁶ and Popovich *et al.*⁹ the direct use of the MMP-spectrum gives overestimation of T_c and the gap function due to a long tail at high energies of the bosonic spectral functions $\sim 1/\omega$. To cure the problem it was proposed to introduce a cut-off or calculate the bosonic self-energy at high energies.³⁸ For simplicity we use the approach of cut-off proposed in ref. 9. A detailed procedure of the calculation is described in Supplementary Note 1.

The plot of T_c vs. $\sqrt{\Gamma}$ is shown in Fig. 3. The solid curve is a theoretical calculation (T_c vs. $\lambda \propto \sqrt{\Gamma}$) based on the Eliashberg theory in which electron correlation effects are substantial. The good agreement of our theory with the experimental data evidences that the magnetic scenario for superconductivity in which Cooper pairing is mediated by spin fluctuations applies to FeSe, and it is likely a universal superconducting mechanism among FeSCs.

Based on our NMR finding that T_c relies only on SFs, the seeming relevance of nematicity with superconductivity may be simply due to the closeness with magnetism, rather than to

superconductivity itself. It should be noted that the strongly anisotropic gap structure^{13–16,22} observed in FeSe may be a natural consequence of the presence of nematicity within the superconducting state. It is because nematicity involves the splitting of d_{xz} and d_{yz} orbitals which should have an inevitable influence on the gap symmetry. However, T_c itself is not necessarily affected by nematicity.³⁹ Nevertheless, nematicity may be considered as an important barometer for superconductivity in FeSCs, as it is strongly coupled to magnetism¹⁸ which in turn directly correlates with superconductivity.

Methods

Crystal growth and characterization. The growth of $\text{Fe}_{1-x}\text{Co}_x\text{Se}$ and $\text{FeSe}_{1-y}\text{S}_y$ single crystals was performed by using the KCl - AlCl_3 flux technique in permanent T-gradient in accordance with refs. 40 and 41. All preliminary operations for the preparation of the reaction mixture were carried out in a dry box with a residual pressure of O_2 and H_2O not higher than 0.1 ppm. At the first stage, polycrystalline samples of the composition $\text{Fe}_{1-x}\text{Co}_x\text{Se}$ and $\text{FeSe}_{1-y}\text{S}_y$ were obtained. For this, Fe, Co, S and Se powders were carefully ground in a mortar in the appropriate ratio, and then annealed in evacuated quartz ampoules at 420 °C for few days. In the second stage, 0.5 g of the prepared sample was placed on the bottom of a thick-walled ampoule, and then the mixture of AlCl_3 and KCl in a molar ratio of $\text{AlCl}_3:\text{KCl} = 2:1$ is added to the ampule, after that the ampule was evacuated and sealed. The sealed ampoule with polycrystalline sample of Fe-Co-Se-S loads was placed in a horizontal 2-zone furnace and heated for five weeks in such a way that, the hot zone temperature was set to 420 °C and the cold zone temperature was set to 370 °C. After five weeks, the furnace was turned off and the ampoule was removed from the furnace. Next, the ampoule was cut and the single crystals from cold zone were separated from the flux by dissolving it in water. The single crystals obtained were thin square plates with metallic luster. The single crystals were grown with platelet like morphology and were characterized by SEM/EDX for compositional analysis.

Nuclear magnetic resonance. ^{77}Se (nuclear spin $I = 1/2$) NMR was carried out in undoped and doped FeSe single crystals at an external magnetic field and in the range of temperature 4.2 – 160 K. The samples were oriented using a goniometer for the accurate alignment along the external field. The ^{77}Se NMR spectra were acquired by a standard

spin-echo technique with a typical $\pi/2$ pulse length 2–3 μs . The nuclear spin-lattice relaxation rate T_1^{-1} was obtained by fitting the recovery of the nuclear magnetization $M(t)$ after a saturating pulse to following fitting function,

$$1 - M(t)/M(\infty) = A \exp(-t/T_1)$$

where A is a fitting parameter that is ideally unity.

Determination of T_c and T_{nem} . The superconducting transition temperature T_c was determined from magnetic susceptibility (χ) measurements by comparing field-cooled and zero-field cooled data, while we obtained the nematic transition temperature T_{nem} by measuring the temperature at which the ^{77}Se NMR line splits (see Fig. 1). Due to the weakness of the signal intensity, we were unable to determine T_c by $(T_1T)^{-1}$ measurements except the undoped FeSe sample. This could give an error in extracting spin fluctuations just above T_c , Γ , which was reflected in an experimental error indicated in Fig. 3.

Data Availability:

The data that support the findings of this study are available from the corresponding author (S.-H. Baek).

Acknowledgments:

We acknowledge A. Chubukov for useful discussions. S.H.B has been supported by the Deutsche Forschungsgemeinschaft (Germany) via DFG Research Grants BA 4927/2-1 and by the National Research Foundation of Korea (NRF-2019R1F1A1057463). D.V.E., B.B., I.M., and S.A. were supported by RSF-DFG project (no. 19-43-04129, BU887/25-1, EF86/7-1). D.V.E and I.M. were also supported by VW foundation in the frame of the VW Trilateral Initiative. S.A. acknowledges financial support from Deutsche Forschungsgemeinschaft (DFG) via Grant No. DFG AS 523/4-1. The work at POSTECH was supported by Institute for Basic Science (no. IBS-R014-D1) and also by the National Research Foundation (NRF) of Korea through the SRC (no. 2018R1A5A6075964) and the Max Planck-POSTECH Center for Complex Phase Materials in Korea (MPK) (no. 2016K1A4A4A01922028). The work of DACH was supported by the program 211 of the Russian Federation Government, agreement No. 02.A03.21.0006, by the Russian Government Program of Competitive Growth of Kazan Federal University.

Competing Interests:

The authors declare no competing financial or non-financial interests.

Author Contributions:

SHB and BB have proposed and initiated the project. JMO, JSK, SA, IM, DC, TU, KT, and YT have grown single crystals and characterized transport and superconducting properties. SHB and JMO performed NMR measurements and analyzed data; SHB, DVE, and BB participated in writing of the manuscript. All authors discussed the results and commented on the manuscript.

Additional information:

Correspondence and requests for materials should be addressed to S.-H. Baek (email: sbaek.fu@gmail.com).

-
- ¹ Fradkin, E., Kivelson, S. A., Lawler, M. J., Eisenstein, J. P. & Mackenzie, A. P. Nematic fermi fluids in condensed matter physics. *Ann. Rev. Cond. Mat. Phys.* **1**, 153–178 (2010).
 - ² Fernandes, R. M., Chubukov, A. V. & Schmalian, J. What drives nematic order in iron-based superconductors? *Nature Phys.* **10**, 97–104 (2014).
 - ³ Böhmer, A. E. & Meingast, C. Electronic nematic susceptibility of iron-based superconductors. *C. R. Physique* **17**, 90–112 (2016).
 - ⁴ Si, Q., Yu, R. & Abrahams, E. High-temperature superconductivity in iron pnictides and chalcogenides. *Nat. Rev. Mater.* **1**, 16017 (2016).
 - ⁵ Yamakawa, Y., Onari, S. & Kontani, H. Nematicity and magnetism in FeSe and other families of Fe-based superconductors. *Phys. Rev. X* **6**, 021032 (2016).
 - ⁶ Chubukov, A. V., Khodas, M. & Fernandes, R. M. Magnetism, superconductivity, and spontaneous orbital order in iron-based superconductors: Which comes first and why? *Phys. Rev. X* **6**, 041045 (2016).
 - ⁷ Kuo, H.-H., Chu, J.-H., Palmstrom, J. C., Kivelson, S. A. & Fisher, I. R. Ubiquitous signatures of nematic quantum criticality in optimally doped Fe-based superconductors. *Science* **352**, 958–962 (2016).

- ⁸ Wang, C. G. *et al.* Electron mass enhancement near a nematic quantum critical point in $\text{NaFe}_{1-x}\text{Co}_x\text{As}$. *Phys. Rev. Lett.* **121**, 167004 (2018).
- ⁹ Wang, F. & Lee, D.-H. The electron-pairing mechanism of iron-based superconductors. *Science* **332**, 200–204 (2011).
- ¹⁰ Dai, P. Antiferromagnetic order and spin dynamics in iron-based superconductors. *Rev. Mod. Phys.* **87**, 855–896 (2015).
- ¹¹ She, J.-H., Lawler, M. J. & Kim, E.-A. Quantum spin liquid intertwining nematic and superconducting order in FeSe. *Phys. Rev. Lett.* **121**, 237002 (2018).
- ¹² Böhmer, A. E. & Kreisel, A. Nematicity, magnetism and superconductivity in FeSe. *J. Phys.: Condens. Matter* **30**, 023001 (2018).
- ¹³ Xu, H. C. *et al.* Highly anisotropic and twofold symmetric superconducting gap in nematically ordered $\text{FeSe}_{0.93}\text{S}_{0.07}$. *Phys. Rev. Lett.* **117**, 157003 (2016).
- ¹⁴ Hashimoto, T. *et al.* Superconducting gap anisotropy sensitive to nematic domains in FeSe. *Nat. Commun.* **9**, 282 (2018).
- ¹⁵ Liu, D. *et al.* Orbital origin of extremely anisotropic superconducting gap in nematic phase of FeSe superconductor. *Phys. Rev. X* **8**, 031033 (2018).
- ¹⁶ Kushnirenko, Y. S. *et al.* Three-dimensional superconducting gap in FeSe from angle-resolved photoemission spectroscopy. *Phys. Rev. B* **97**, 180501 (2018).
- ¹⁷ Hosoi, S. *et al.* Nematic quantum critical point without magnetism in $\text{FeSe}_{1-x}\text{S}_x$ superconductors. *Proc. Natl. Acad. Sci. U.S.A.* **113**, 8139–8143 (2016).
- ¹⁸ Matsuura, K. *et al.* Maximizing T_c by tuning nematicity and magnetism in $\text{FeSe}_{1-x}\text{S}_x$ superconductors. *Nat. Commun.* **8**, 1143 (2017).
- ¹⁹ Imai, T., Ahilan, K., Ning, F. L., McQueen, T. M. & Cava, R. J. Why does undoped FeSe become a high- T_c superconductor under pressure? *Phys. Rev. Lett.* **102**, 177005 (2009).
- ²⁰ Sun, J. P. *et al.* High- T_c superconductivity in FeSe at high pressure: dominant hole carriers and enhanced spin fluctuations. *Phys. Rev. Lett.* **118**, 147004 (2017).
- ²¹ Wiecki, P. *et al.* Persistent correlation between superconductivity and antiferromagnetic fluctuations near a nematic quantum critical point in $\text{FeSe}_{1-x}\text{S}_x$. *Phys. Rev. B* **98**, 020507 (2018).
- ²² Rhodes, L. C. *et al.* Scaling of the superconducting gap with orbital character in FeSe. *Phys. Rev. B* **98**, 180503 (2018).
- ²³ Wang, P. S. *et al.* Robust short-range-ordered nematicity in FeSe evidenced by high-pressure

- NMR. *Phys. Rev. B* **96**, 094528 (2017).
- ²⁴ Wiecki, P. *et al.* NMR evidence for static local nematicity and its cooperative interplay with low-energy magnetic fluctuations in FeSe under pressure. *Phys. Rev. B* **96**, 180502 (2017).
- ²⁵ Kuwayama, T. *et al.* ⁷⁷Se-NMR study under pressure on 12%-S doped FeSe. *J. Phys. Soc. Jpn.* **88**, 033703 (2019).
- ²⁶ Baek, S.-H. *et al.* Orbital-driven nematicity in FeSe. *Nature Mater.* **14**, 210–214 (2015).
- ²⁷ Baek, S.-H. *et al.* Nematicity and in-plane anisotropy of superconductivity in β -FeSe detected by ⁷⁷Se nuclear magnetic resonance. *Phys. Rev. B* **93**, 180502 (2016).
- ²⁸ Ok, J. M. *et al.* Nematicity and magnetism in LaFeAsO single crystals probed by ⁷⁵As nuclear magnetic resonance. *Phys. Rev. B.* **97**, 180405 (2018).
- ²⁹ Urata, T. *et al.* Superconductivity pairing mechanism from cobalt impurity doping in FeSe: Spin (s_{\pm}) or orbital (s_{++}) fluctuation. *Phys. Rev. B* **93**, 014507 (2016).
- ³⁰ Abdel-Hafez, M. *et al.* Impurity scattering effects on the superconducting properties and the tetragonal-to-orthorhombic phase transition in FeSe. *Phys. Rev. B* **93**, 224508 (2016).
- ³¹ Coldea, A. I. *et al.* Evolution of the Fermi surface of the nematic superconductors FeSe_{1-x}S_x. arXiv:1611.07424 (unpublished).
- ³² Massat, P. *et al.* Collapse of critical nematic fluctuations in FeSe under pressure. *Phys. Rev. Lett.* **121**, 077001 (2018).
- ³³ Lederer, S., Schattner, Y., Berg, E. & Kivelson, S. A. Enhancement of superconductivity near a nematic quantum critical point. *Phys. Rev. Lett.* **114**, 097001 (2015).
- ³⁴ Allen, P. B. & Mitrović, B. Theory of superconducting T_c . *Solid State Physics* **37**, 1–92 (1983).
- ³⁵ Millis, A. J., Monien, H. & Pines, D. Phenomenological model of nuclear relaxation in the normal state of YBa₂Cu₃O₇. *Phys. Rev. B* **42**, 167–178 (1990).
- ³⁶ Radtke, R. J., Ullah, S., Levin, K. & Norman, M. R. Constraints on superconducting transition temperatures in the cuprates: Antiferromagnetic spin fluctuations. *Phys. Rev. B* **46**, 11975–11985 (1992).
- ³⁷ Popovich, P. *et al.* Specific heat measurements of Ba_{0.68}K_{0.32}Fe₂As₂ single crystals: evidence for a multiband strong-coupling superconducting state. *Phys. Rev. Lett.* **105**, 027003 (2010).
- ³⁸ Abanov, A., Chubukov, A. V. & Schmalian, J. Quantum-critical theory of the spin-fermion model and its application to cuprates: normal state analysis. *Adv. Phys.* **52**, 119–218 (2003).
- ³⁹ Kang, J., Fernandes, R. M. & Chubukov, A. Superconductivity in FeSe: the role of nematic

order. *Phys. Rev. Lett.* **120**, 267001 (2018).

⁴⁰ Chareev, D. *et al.* Single crystal growth and characterization of tetragonal FeSe_{1-x} superconductors. *CrystEngComm* **15**, 1989–1993 (2013).

⁴¹ Chareev, D. *et al.* Single crystal growth, transport and scanning tunneling microscopy and spectroscopy of FeSe_{1-x}S_x. *CrystEngComm* **20**, 2449–2454 (2018).

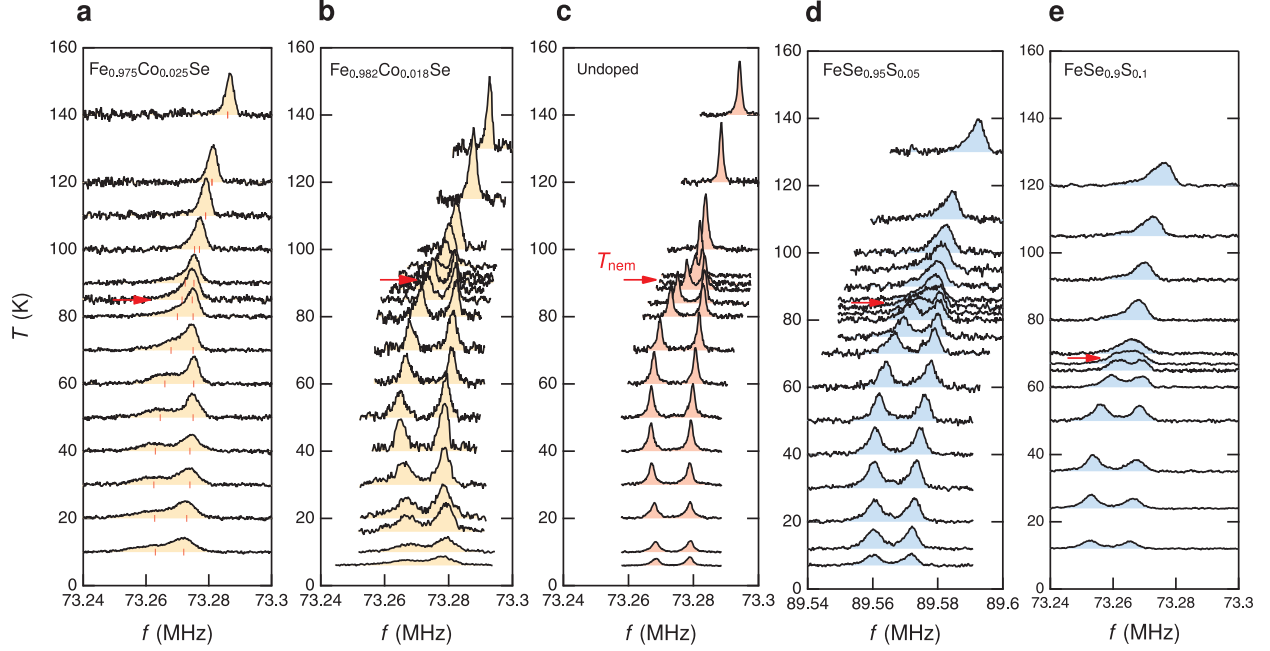


FIG. 1. ^{77}Se NMR spectra in undoped and doped FeSe single crystals for $H \parallel a$. **a-b**, Temperature dependence of ^{77}Se spectrum of $\text{Fe}_{1-x}\text{Co}_x\text{Se}$. For $x = 0.018$ (**b**), the ^{77}Se spectrum shows a very similar behavior as the undoped one, except a moderate line broadening. For a slightly larger doping, $x = 0.025$ (**a**), the ^{77}Se line undergoes a considerable line broadening. While the splitting of the two ^{77}Se lines were clearly identified at low temperatures (vertical bars), the onset of the splitting is not well defined, being ascribed to local disorder. **c**, Temperature dependence of ^{77}Se spectrum for undoped FeSe. **d-e**, Temperature dependence of ^{77}Se spectrum of $\text{FeSe}_{1-y}\text{S}_y$ for $y = 0.05$ and 0.1 , respectively. T_{nem} is progressively suppressed with increasing S doping.

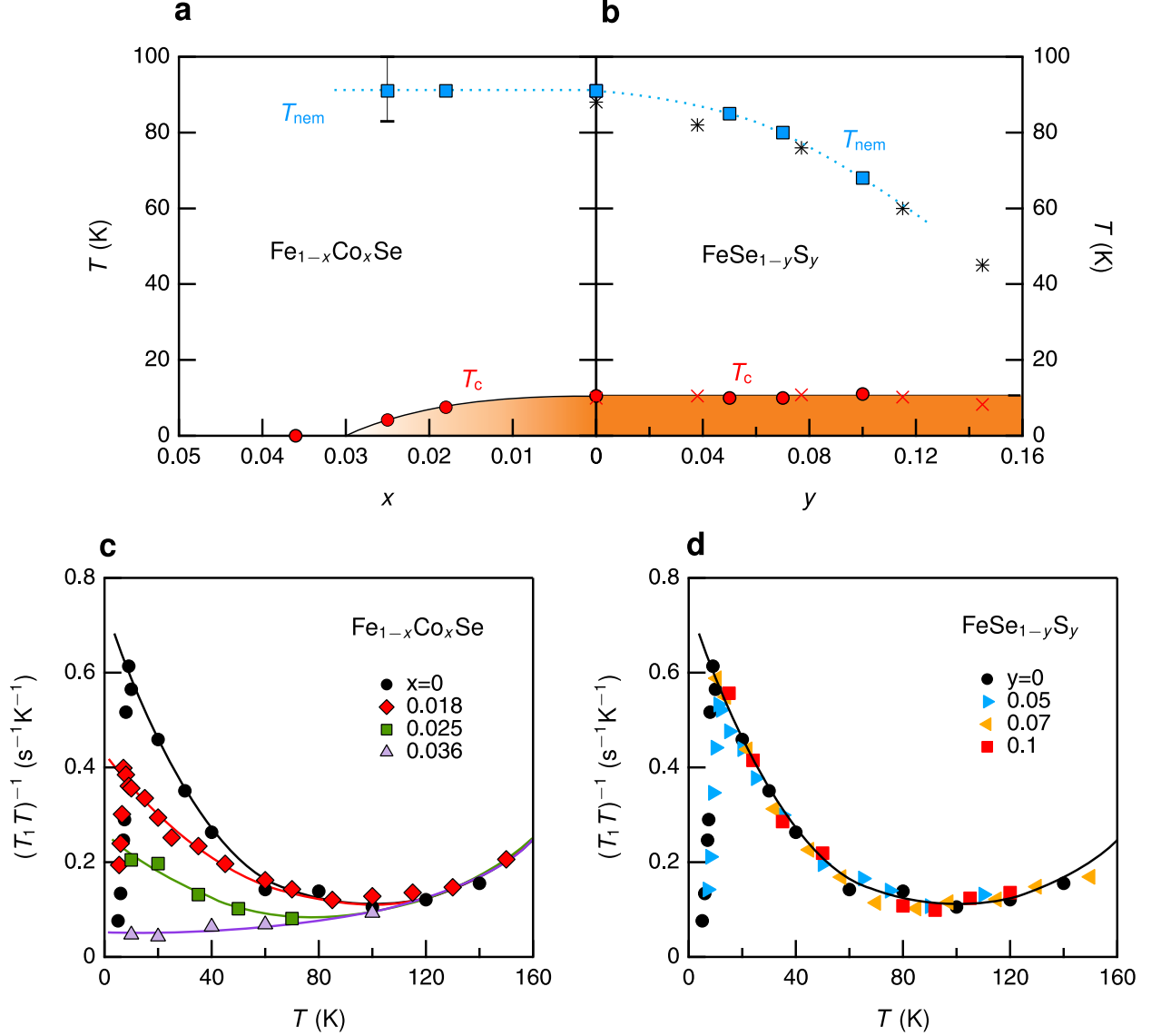


FIG. 2. Doping dependence of spin fluctuations for $H \parallel a$ in FeSe. **a** and **b**, The phase diagrams of $Fe_{1-x}Co_xSe$ and $FeSe_{1-y}S_y$, respectively. For Co doping, T_{nem} is hardly influenced, but T_c is strongly suppressed. In contrast, for S doping, T_{nem} is suppressed with increasing y and T_c remains nearly the same. The asterisk(*) and cross (\times) symbols are the T_{nem} and T_c data, respectively, extracted from Ref. 17. **c**, The spin-lattice relaxation rate divided by temperature, $(T_1 T)^{-1}$ which measures spin fluctuations, as a function of temperature and Co-doping x in $Fe_{1-x}Co_xSe$. The enhancement of $(T_1 T)^{-1}$ at low temperatures is progressively suppressed with increasing x (see Fig. 3). The solid lines are guides to the eyes. **d**, $(T_1 T)^{-1}$ as a function of temperature and S-doping y in $FeSe_{1-y}S_y$. Spin fluctuations are unchanged with increasing S doping y , being consistent with T_c that is nearly independent of y .

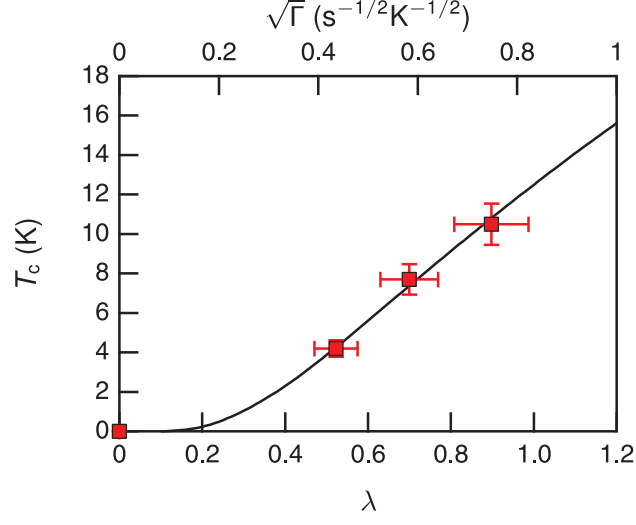


FIG. 3. Superconducting transition temperature T_c vs. $\sqrt{\Gamma}$, where Γ is the strength of spin fluctuations just above T_c for $H_{\parallel a}$ in Co-doped FeSe single crystals. The solid line represents our theory of T_c vs. the coupling constant $\lambda \propto \sqrt{\Gamma}$ (see text). The error bars represent the uncertainty in determining T_c and Γ .

Supplementary Material to “Separate tuning of nematicity and spin fluctuations to unravel the origin of superconductivity in FeSe”

Supplementary Note 1. Superconducting critical temperature in the strong coupling approximation.

The superconducting critical temperature T_c in the framework of the Eliashberg theory is given by the solution of the system of the linearized Eliashberg equations:^{1,2}

$$Z_{\alpha n} = 1 + T_c \sum_{\omega'_{n'}, \beta} \lambda_{\alpha\beta}^z(n - n') \frac{\text{sign}(\omega_{n'})}{\omega_n}, \quad (3)$$

$$Z_{\alpha n} \Delta_{\alpha n} = T_c \sum_{\omega'_{n'}, \beta} \lambda_{\alpha\beta}^\phi(n - n') \frac{\Delta_{\beta n'}}{\omega_{n'}}. \quad (4)$$

where $\omega_n = \pi T_c(2n + 1)$ are the Matsubara frequencies, $\Delta_{\alpha n}$ are the gap functions, $Z_{\alpha n}$ are the Z functions, and α, β are the band indices. The coupling functions

$$\lambda_{\alpha\beta}^{\tilde{\phi}, z}(n - n') = 2\lambda_{\alpha\beta}^{\tilde{\phi}, z} \int_0^\infty d\Omega \frac{\Omega B(\Omega)}{[(\omega_n - \omega_{n'})^2 + \Omega^2]} \quad (5)$$

are expressed through the normalized bosonic spectral function $B(\Omega)$. For the sake of simplicity we neglect the intraband interaction ($\lambda_{11}^{\phi, z} = \lambda_{22}^{\phi, z} = 0$). The interband coupling constants $\lambda_{\alpha\beta}^{\tilde{\phi}}$ are chosen to be negative (repulsive) due to the prevailing spin-fluctuation mechanism of the electron-electron interaction.^{3,4} The matrix elements $\lambda_{\alpha\beta}^z$ are positive. For simplicity we use the approximation $\lambda_{\alpha\beta}^z = |\lambda_{\alpha\beta}^{\tilde{\phi}}| \equiv |\lambda_{\alpha\beta}|$ and neglects the \mathbf{k} -space anisotropy in the gap functions $\Delta_{\alpha n}$.

a. Spin-fluctuation model. A phenomenological model of spin fluctuation spectra based on NMR data was proposed for nearly antiferromagnetic metals by Millis et al.⁵ [Millis-Monien-Pines (MMP) model]. They argued that the low energy dynamical spin susceptibility may be represented in the following form:

$$\text{Im}\chi(\mathbf{q}, \omega) = \frac{\chi_0 \Gamma_{\text{sf}}}{\pi \omega_{\text{sf}}} \frac{(\omega/\omega_{\text{sf}})}{(1 + \xi^2 |\mathbf{q} - \mathbf{Q}|^2)^2 + (\omega/\omega_{\text{sf}})^2} \times \Theta(\Omega_c - |\omega|), \quad (6)$$

where Q is the nesting vector, Ω_c is the energy cut-off and

$$\omega_{\text{sf}} = \Gamma_{\text{sf}} \frac{a^2}{\pi^2 \xi^2},$$

where ξ is the correlation length, characterizing the the proximity to the antiferromagnetic instability. At the transition point it diverges $\xi^{-1} = 0$. The static spin susceptibility is

denoted as χ_0 , a is the lattice constant, and Γ_{sf} is the frequency scale characterizing the spin fluctuations. Within this model one gets the spin lattice relaxation rate in the following form at low temperatures (see also ref. 6.):

$$\Gamma = \frac{1}{T_1 T} = \gamma_g^2 \lim_{\omega \rightarrow 0} \sum_{\mathbf{q}} \frac{M^2 \chi''(\mathbf{q}, \omega)}{\omega} \sim \frac{\chi_0}{\xi^{-2}}. \quad (7)$$

b. Boson spectral function. The main input into the Eliashberg equations Eqs.(3) and (4) is the spectral function of the intermediate bosons $B(\mathbf{q}, \omega)$:

$$\alpha^2 F(\omega) = \frac{\sum_{\mathbf{k}, \mathbf{k}'} \delta(\epsilon_{\mathbf{k}}) \delta(\epsilon_{\mathbf{k}'}) |A(\mathbf{k}, \mathbf{k}')|^2 B(\mathbf{k} - \mathbf{k}', \omega)}{\sum_{\mathbf{k}} \delta(\epsilon_{\mathbf{k}})} \quad (8)$$

where $A(\mathbf{k}, \mathbf{k}')$ is the matrix element for the scattering an electron in Bloch state \mathbf{k} to \mathbf{k}' and

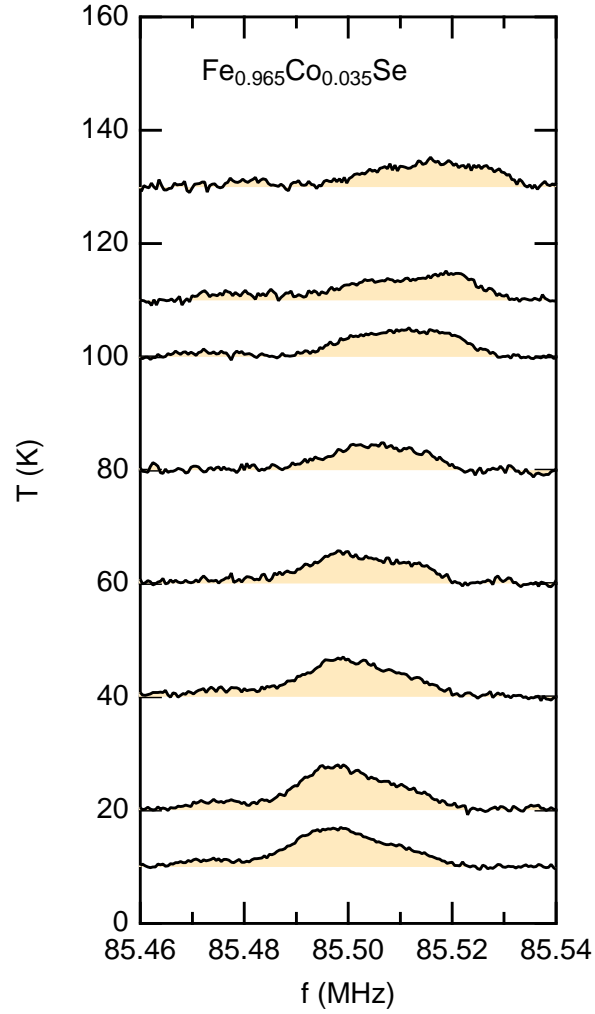
$$B(\mathbf{q}, \Omega) = -\frac{1}{\pi} N(0) \text{Im} \chi(\mathbf{q}, \Omega) \quad (9)$$

is the spectral function of the spin fluctuations normalized by the density of states at the Fermi level $N(0)$. As it was pointed out in refs. 7–9, that use of the MMP spectrum in the Eliashberg equation leads to overestimation of T_c and superconducting gaps due to a long tail at high frequencies $\propto 1/\omega$. Here, we adopt the phenomenological approach proposed by Popovich et al.⁹ The low energy part of the bosonic function is given by Eq. (6) and the function decays fast after a characteristic cut-off energy. The cut-off energy is determined by the band structure and in the leading approximation can be taken independent on the distance to the quantum critical point.

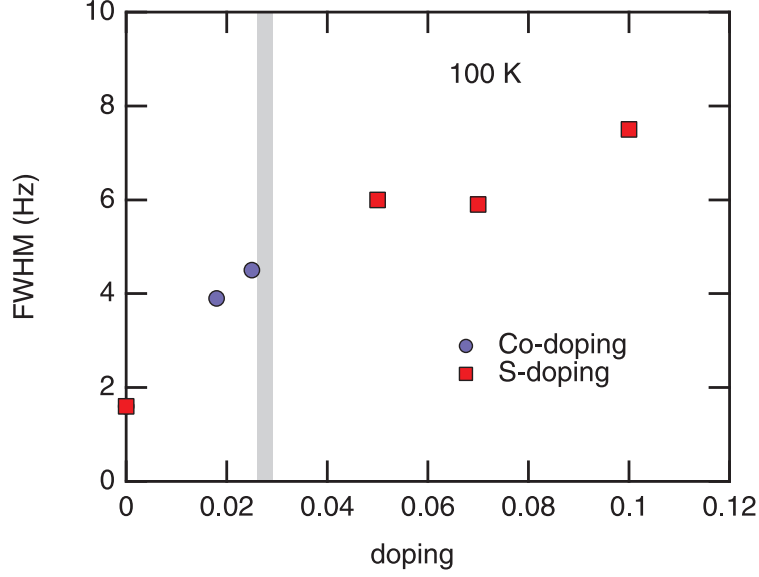
Since we consider the leading term, we neglect the momentum dependence of $A = g = \text{const}$. Performing the momentum integration in Eq. (8) we get for small ω :

$$\alpha^2 F(\omega) \approx \frac{g^2 N(0)}{4\pi^2 (\xi/a)} \frac{\omega}{\omega_{\text{sf}}} \sim g^2 N(0) \frac{\xi}{a} \frac{\omega}{\Gamma_{\text{sf}}}. \quad (10)$$

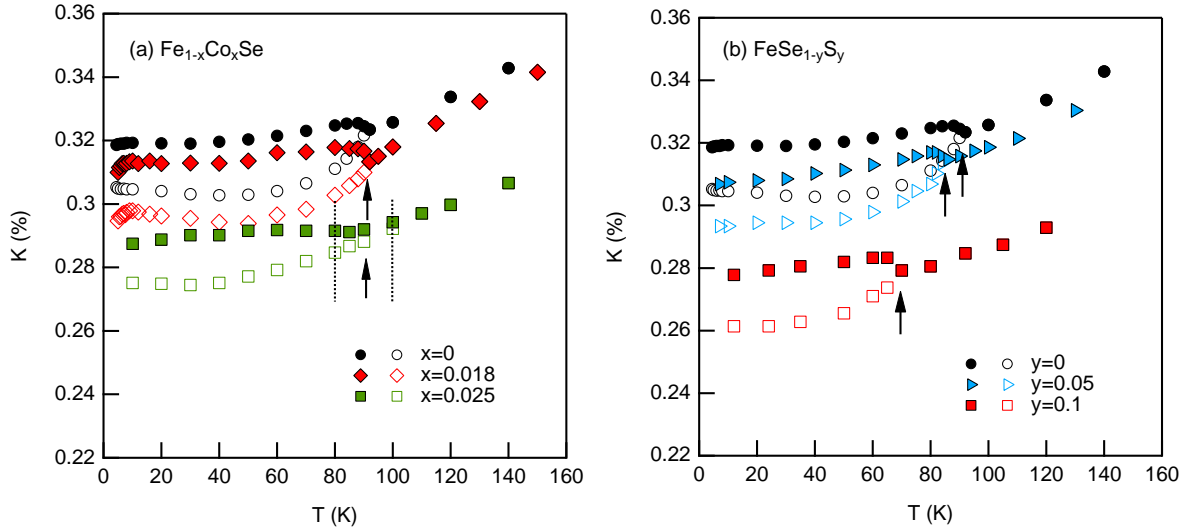
It determines that $\lambda \sim \xi \sim \sqrt{\Gamma}$. In Fig. 3 of the main text we show the experimental and calculated T_c vs. λ and $\sqrt{\Gamma}$ correspondingly. The fit gives the scale of the coupling constants.



Supplementary Figure 1. Temperature dependence of ^{77}Se spectrum at 3.6%Co doping. The full-width-at-half-maximum (FWHM) significantly increased at this doping. Since the splitting of the line due to nematicity is smaller than the FWHM, T_{nem} cannot be identified.



Supplementary Figure 2. Doping dependence of ^{77}Se full-width-at-half-maximum (FWHM) at 100 K. The gray line denotes the existence of a critical Co doping.



Supplementary Figure 3. ^{77}Se Knight shift data in (a) $\text{Fe}_{1-x}\text{Co}_x\text{Se}$ (b) $\text{FeSe}_{1-y}\text{S}_y$. The arrow indicates the nematic transition temperature T_{nem} . For $x = 0.025$ in (a), T_{nem} cannot be identified accurately, but is in the range 80-100 K. It should be noted that the Knight shift splitting $\Delta\mathcal{K}(T)$ is sensitive to an inevitable slight misalignment of the sample with respect to H . Therefore, we attribute the small variation of $\Delta\mathcal{K}(T)$ with doping to an experimental error.

-
- ¹ Allen, P. B. & Mitrović, B. *Solid State Physics* **37**, 1 (1982).
- ² Efremov, D. V., Drechsler, S.-L., Rosner, H., Grinenko, V. & Dolgov, O. V. A multiband Eliashberg-approach to iron-based superconductors. *physica status solidi (b)* **254**, 1600828 (2017).
- ³ Chubukov, A. V., Efremov, D. V. & Eremin, I. Magnetism, superconductivity, and pairing symmetry in iron-based superconductors. *Phys. Rev. B* **78**, 134512 (2008).
- ⁴ Mazin, I. I. & Johannes, M. D. A key role for unusual spin dynamics in ferropnictides. *Nat. Phys.* **5**, 141–145 (2009).
- ⁵ Millis, A. J., Monien, H. & Pines, D. Phenomenological model of nuclear relaxation in the normal state of $\text{YBa}_2\text{Cu}_3\text{O}_7$. *Phys. Rev. B* **42**, 167–178 (1990).
- ⁶ Millis, A. J. Nearly antiferromagnetic Fermi liquids: An analytic Eliashberg approach. *Phys. Rev. B* **45**, 13047 (1992).
- ⁷ Schüttler, H.-B. & Norman, M. R. Contrasting dynamic spin susceptibility models and their relation to high-temperature superconductivity. *Phys. Rev. B* **54**, 13295–13305 (1996).
- ⁸ Benfatto, L., Cappelluti, E. & Castellani, C. Spectroscopic and thermodynamic properties in a four-band model for pnictides. *Phys. Rev. B* **80**, 214522 (2009).
- ⁹ Popovich, P. *et al.* Specific heat measurements of $\text{Ba}_{0.68}\text{K}_{0.32}\text{Fe}_2\text{As}_2$ single crystals: evidence for a multiband strong-coupling superconducting state. *Phys. Rev. Lett.* **105**, 027003 (2010).